ELSEVIER

Journal of Hazardous Materials 141 (2007) 591–606

Journal of Hazardous Materials

www.elsevier.com/locate/jhazmat

Release of Zn, Ni, Cu, SO_4^{2-} and CrO_4^{2-} as a function of pH from cement-based stabilized/solidified refinery oily sludge and ash from incineration of oily sludge

Athanasios K. Karamalidis [1], Evangelos A. Voudrias *

Department of Environmental Engineering, Democritus University of Thrace, GR 671 00 Xanthi, Greece

Received 14 February 2006; received in revised form 30 June 2006; accepted 11 July 2006
Available online 21 July 2006

Abstract

A framework for the evaluation of leaching behavior of inorganic constituents from stabilized/solidified refinery oily sludge and ash produced from incineration of oily sludge with cement was employed. Metal and anion release as a function of pH was investigated. The leaching test consisted of multiple parallel extractions at pH range from 2 to 12. Remarkably good immobilization >98% was observed for metals of solidified ash at pH > 6 and >93% of solidified oily sludge at pH > 7. Sulfate leaching was high at pH range 2–12. The leaching behavior of metals and anions was simulated by VMINTEQ. The calculations showed that leaching behavior of Zn, Ni and Cu was controlled by chemical equilibrium and surface complexation onto ferrihydrite, at the pH range 2–12. The dominant solid phases that controlled metal leachability were metal hydroxides. The dominant mechanism that described sulfate leaching was found to be chemical equilibrium. Sulfate and also chromate leachability was controlled by Ettringite and Cr(VI)Ettringite as the major minerals affecting their release.

Keywords: Refinery oily sludge; Incinerated oily sludge; Cement; Leaching; Metal; Anion; Stabilization/solidification; Sorption; Surface complexation

1. Introduction

Many leaching tests have been developed, evaluated and applied to a variety of materials and waste for regulatory purposes, waste management, environmental impact assessment and for scientific purposes [1,2]. Toxicity Characteristic Leaching Procedure (TCLP) is a leaching test that has been used for most of these purposes. Although TCLP is one of the most widely used leaching tests, it has come to unfavorable criticism. There are limitations of using the TCLP for simulating the leaching of contaminants in landfills. These limitations have resulted in legal challenges concerning the failure of the US EPA to provide adequate justification for specifying the TCLP for the classification of several industrial wastes [3]. Recent studies have shown that the TCLP may not accurately measure the ability for arsenic to migrate from a landfill [4]. Poon and Lio [5] has reported TCLP limitations and the EPA Science Advisory Board criticized the protocol on the basis of several technical considerations, such as leaching kinetics, liquid to solid ratio, pH, potential of colloid formation, particle size reduction, aging, volatile losses, and codisposal with other waste [6]. In the present study, an alternative to TCLP framework was used for the evaluation of leaching of inorganic constituents from stabilized/solidified oily sludge and ash. This alternative was a leaching test for alkalinity, solubility and release of metals and anions as a function of pH [6].

A metal ion may be immobilized into the cement matrix. It may either be bound in the alkaline cement matrix as an oxide or mixed oxide, be sorbed to surfaces, or be incorporated into cement minerals [7]. Recently, incorporation of Zn to the interlayer or sorption to internal surface of Calcium Silicate Hydrate (CSH; $CaOSiO_2{\cdot}xH_2O$) which is a mineral formed during cement hydration, have been proved [8–10]. Surface complexation modeling, with a modified triple layer model, was used to describe Zn sorption onto ferrihydrite ($Fe(OH)_{3(s)}$) [11]. Zhu has estimated surface precipitation constants for sorption of divalent metals M^{2+} (e.g. Ni^{2+}, Cu^{2+}, Zn^{2+}) onto ferrihydrite, and concluded that surface complexation dominates sorption at

* Corresponding author. Tel.: +30 25410 79377; fax: +30 25410 79376.
E-mail addresses: akaramal@env.duth.gr (A.K. Karamalidis), voudrias@env.duth.gr (E.A. Voudrias).
[1] Tel.: +30 25410 79395; fax: +30 25410 79376.

0304-3894/$ – see front matter © 2006 Elsevier B.V. All rights reserved.
doi:10.1016/j.jhazmat.2006.07.034

low dissolved metal concentrations [12]. Ni uptake by blended cement has been attributed to the formation of a 4:1 Ca:Ni phase, which was thought to replace $Ni(OH)_2$ as the solubility-limiting phase in cement systems. However, X-ray diffraction of Ni-doped cement pastes showed only the presence of a poorly crystallized $Ni(OH)_2$ gel [13]. Under highly alkaline conditions, Ni–Al–oxyhydroxides were potential host phases for Ni in cement, but, nevertheless, $Ni(OH)_2$ was present to some extent [13]. The pH-dependent adsorption and coprecipitation of Cu with the hydrous oxides of Fe and Al were previously reported by Karthikeyan et al. [14]. They also applied a generalized two-layer model on Cu adsorption onto ferrihydrite over a range of pH and surface loading conditions, and found that it was satisfactory for low sorbate/sorbent ratios where metal oxide interaction is adequately described as Cu^{2+} coordination to surface functional groups [15].

Another mineral affecting metal immobilization in the cement matrix is Ettringite ($Ca_6[Al(OH)_6]_2(SO_4)_3{\cdot}26H_2O$), because of its abundance and appropriate structure [7,16]. Several publications [17–19] showed that Ettringite is one of those minerals that can contain in its structure anions and oxyanions as well as cations. Anion substitution in Ettringite can take place either by reacting with surface sites (ligand exchange) or by substituting inside the channels for sulfate (isomorphic substitution) [14,18]. Anionic substituted Ettringites have been reported and synthesized for AsO_4^{3-}, $B(OH)_4^-$, CO_3^{2-}, CrO_4^{2-}, NO_3^-, OH^-, SeO_4^{2-}, SO_3^{2-}, and VO_4^{3-}. In cementitious material, $B(OH)_4^-$, CrO_4^{2-}, MoO_4^{2-}, SeO_4^{2-}, and SO_3^{2-} also have been shown to serve as interlayer anions [17]. In such cement-matrices, because of their high alkaline environment, it is common that chromium speciation is dominated by CrO_4^{2-} above pH 8 [20]. Ettringite can also be found in cement-related materials, such as in cement-solidified waste. Contrary to substitution, at extremely low concentrations, below the threshold for precipitation, contaminant availability tends to be controlled by sorption mechanisms [21].

In this study, the leaching behavior of metals and anions released from solidified/stabilized refinery oily sludge and ash produced by incineration of refinery oily sludge, was examined by means of the alkalinity, solubility and release as a function of pH test. Refinery oily sludge and ash are classified as hazardous wastes. Metals and anions, contained in such waste are potential contaminants to groundwater and soil. Cement-based stabilization/solidification is a low cost treatment process, which has been widely applied to waste containing radioactive contaminants, heavy metals, and other hazardous substances. In some cases treatment technologies, such as incineration, are not a feasible option, either because of unavailable infrastructure or of high cost. Thus, alternative treatment technologies must be applied. Stabilization/solidification aiming to landfill disposal is certainly one of them. Data about metal and anion leaching from real refinery oily sludge and incinerated refinery sludge, stabilized/solidified with II-45 ordinary Portland cement (OPC) as a function of pH, are scarce or do not exist. Much work has been done about leachability of metals using the TCLP protocol, but because of its recent criticism, in this work a new leaching framework [6] was applied. The work focuses on the immobilization mechanisms, which control the leaching behavior of metals and anions. For this purpose, in addition to leaching experiments, the computer program Visual MINTEQ was employed. Metals were assumed to be mainly in the form of hydroxides and simulated by chemical equilibrium and surface complexation using diffuse layer model (DLM). Sulfate leaching was simulated by chemical equilibrium and chromate by chemical equilibrium and surface complexation. Cr(VI)Ettringite, Ettringite, $ZnSO_{4(s)}$, and $Fe_2(SO_4)_{3(s)}$ were considered for sulfate leaching and $CaCrO_{4(s)}$ for chromate leaching.

2. Materials and methods

2.1. Oily sludge and incinerated oily sludge

Sludge samples were obtained from a Greek refinery (R). The R samples originated from a centrifuge unit, which contained a mixture of different kinds of oily sludge, such as API type gravity separator sludge and dissolved air flotation (DAF) sludge. The purpose of the centrifuge unit was to recover and reuse the hydrocarbon fraction contained in the sludge. The incinerated oily sludge (IR) (ash) was produced by incineration of the R samples in a laboratory kiln.

2.2. Binding materials

The ordinary Portland cement (OPC), II-45, was obtained from TITAN Cement Company SA. The II-45 OPC contains pozzolanic material (natural pozzolan 7%, w/w). The chemical composition of the cement and its pozzolanic component was determined by XRF analysis (Table 1). For the stabilization/solidification (S/S) process, ultra-pure water was used in order to minimize contamination of the solidified specimens by constituents contained in the water. Ultra-pure water (ASTM Type I, ISO 3696) was prepared using the system USF-ELGA, UHQ II.

2.3. Incineration procedure

Measured amounts of R oily sludge samples were placed into a stainless steel container, capable of resisting temperature above 1200 °C, without being disintegrated. The temperature of

Table 1
Chemical composition of II-45 OPC and natural pozzolan contained in II-45 OPC, determined by XRF analysis

Component	II-45 OPC (wt.%)	Natural pozzolan of II-45 OPC (wt.%)
SiO_2	28.3	64
Al_2O_3	8.7	14
Fe_2O_3	3.6	5
CaO	50.8	7
MgO	2.2	1.5
K_2O	2.0	2.5
SO_3	3.2	–
Lost on ignition		5
Total	98.8	99

incineration was set at 950 °C. The kiln was not pre-heated, to avoid self-ignition of the waste. The samples were incinerated for 2 h, then, they were let gradually cool and particle reduced. After mixing, the samples were incinerated for two additional hours. The characterization of the incinerated oily sludge (ash) showed that total solids were 99.9% (standard deviation; S.D.: ±0.01) and 0.1% (S.D.: ±0.001) moisture (on wet weight basis). The remainder of the parameters were: COD (chemical oxygen demand) (mg O_2/g): 0, VS (volatile solids): 0% and FS (fixed solids): 100%, on dry weight basis. The analytical methods used for determination of the above parameters were according to Standard Methods [22].

2.4. Stabilization and solidification

Measured amounts of OPC were added to known amount of incinerated sludge or oily sludge, followed by addition of ultra-pure water at water to binder ratio of approximately 0.4. The slurries were mixed manually, using a plastic bowl and a rubber spatula. After mixing, the slurries were poured into plastic cylindrical molds. Air bubbles in the paste were removed by tapping the mold with approximately 40 hits (for about 1 min). The molds then were exposed to ambient air. The samples were cured at approximately 24 °C in the laboratory for 28 days. The cured samples were demolded and ground to pass through a 100 μm sieve before used in the release as a function of pH leaching test. The total weight of a solidified sample is given by $T = W + B + W_a$, where T is the total weight (g) of the S/S specimen, W is the waste wet weight (g) which has been used for every S/S specimen, B is the weight (g) of the binder additive and W_a is the added water (g). The value of B is given by $B = [(B\%)W]/100$ and $(B\%)$ is the percentage of the binder added with respect to the sludge wet weight. The amount of OPC used in all S/S experiments varied from 10% to 50% with respect to the wet weight of sludge, as it is shown in Table 2.

2.5. Alkalinity, solubility and release as a function of pH leaching test

The alkalinity, solubility and release as a function of pH leaching test consists of 11 parallel extractions of particle size reduced material at a liquid to solid (L/S) ratio of 10 mL extractant/g dry sample. An acid or base addition schedule was formulated for 11 extracts with final solution pH values between 2 and 12 through addition of aliquots of 2 mol/L HNO_3 or 1 mol/L KOH as needed [6]. The natural pH of the sample was included in the titration schedule, as one of the parallel extractions. In some cases, where more detailed description of the solubility was necessary, more than 11 parallel extractions were conducted.

A preliminary pH titration test was used in order to decide the final titration schedule. A sample mass of 8 g dry sample was added in ultra-pure water at L/S ratio of 100 mL/g dry sample at room temperature of 20 ± 2 °C. The natural pH of the sample was measured after 25 min of stirring and 5 min of settling. Depending on the natural pH of the sample small aliquots of 100–500 μL acid (2 mol/L) or base (1 mol/L) were added, as required to formulate a titration curve. The titration curve covered the range from pH 1.5 to 13 and showed the pH response as a function of the equivalents of acid or base added per dry gram of sample.

Then, a known amount of sample was placed into borosilicate glass bottles, ultra-pure water was added at L/S ratio of 10 mL/g dry sample and acid or base was added according to the pH target. The bottles were tumbled in an end-over-end fashion at 28 ± 2 rpm for a period of 48 h. Afterwards, the bottles were allowed to settle for 1 h and a small fraction of the supernatant leachate was transferred to a beaker for pH determination. The remainder of the leachate was separated from the solid by vacuum filtration through 0.45 μm polypropylene filtration membranes. Analytical samples of leachates were collected for metal determination.

The pH values of the stabilized/solidified samples and their leachates were determined using a InoLab Level 2 WTW pH meter and a SenTix 60 glass electrode calibrated with buffer solutions at pH values 4, 7 and 10.

2.6. Acid neutralizing capacity test

The oily sludge was ground to pass a 150 μm sieve. Oily sludge was subdivided into 11 sub-samples, each of 3 g in weight. Each sub-sample was placed in an Erlenmeyer flask

Table 2
Detailed description of sample mixtures

Mixture name	Oily sludge (g)	Incinerated oily sludge (g)	II-45 OPC addition (g)	Actual % of cement in the specimens
R	100	–	–	–
IR	–	100	–	–
II-45 CS[a]	–	–	100	100
R II-45 30%[b]	100	–	30	23.1
R II-45 40%	100	–	40	28.6
R II-45 50%	100	–	50	33.3
IR II-45 30%	–	100	30	23.1
IR II-45 40%	–	100	40	28.6
IR II-45 50%	–	100	50	33.3

[a] Cement sample.
[b] 30% = (30 g cement/100 g waste) × 100.

Table 3
Concentrations of metals in the oily sludge and ash

Metal	Dry weight oily sludge (mg/kg)	Dry weight ash (mg/kg)	Dry weight II-45 cement (mg/kg)
Fe	282,936 (3.5)[a]	288,445 (5.5)	
Cu	719 (10.4)	1317 (4.3)	39
Co	ND[b]	ND	11
Cd	ND	ND	1
Cr	222 (8.2)	607 (8.5)	35
Pb	119 (7.8)	242 (21.6)	8
Ni	192 (6.1)	832 (8.3)	89
Zn	1000 (1.6)	1529 (2.5)	120

[a] The numbers in parenthesis are %R.S.D. ($n = 6$).
[b] Not detected.

and an increasing amount of nitric acid (2 mol/L) was added in each successive flask. The flasks then were tumbled strongly at room temperature for 48 h to reach equilibrium. At this point, the pH was measured [5]. In order to maintain sample integrity, drying of the oily sludge was deemed inappropriate. In such a case, volatile organic loss and altering the original structure of the solid would have occurred.

2.7. Determination of metal concentration

Prior to analysis, all samples were prepared according to method 3050B USEPA [23]. Concentrations of Zn, Fe, Ni, Cu, and Cr were determined by flame atomic absorption spectrophotometry (Varian, SpectrAA 220). Where strong matrix effects arose because of the nature of the incinerated or oily sludge, metal concentrations were determined using the *Standard Addition Method* [24]. The determination of metals in oily sludge and ash is presented in Table 3. As expected, metal concentration was higher in ash than in sludge. The concentration of Fe was very high in both wastes. The presence of Fe is important with respect to immobilization of metals, due to their sorption onto iron oxides. Co and Cd were not detected.

2.8. Determination of anion concentration

An ion chromatography method was developed to determine the concentration of the following anions: F^-, Cl^-, NO_2^-, Br^-, PO_4^{3-}, SO_4^{2-}, SCN^- and the oxyanions CrO_4^{2-}, MoO_4^{2-} and SeO_4^{2-}. From these anions only SO_4^{2-}, CrO_4^{2-} and in some cases F^- and Cl^- were detected in the extracts. The addition of high concentration of nitric acid in these extracts prevented the determination of NO_3^- originally present in the leachate. For anion determination an ion-suppressed chromatography was employed. The high pressure liquid chromatography (HPLC) system consisted of an anion suppressor (DS-Plus Alltech), an anion separation column (Allsep anion 7 μm, Alltech) and a conductivity detector (550 conductivity detector, Alltech). The eluent was 0.85 mM $NaHCO_3$/0.9 mM Na_2CO_3 at a flow rate of 1.2 mL/min at 35 °C. The same temperature (35 °C) was used for the detector. The injection volume was 20 μL. A four-point calibration was used and calibration curves were developed with $r^2 = 0.993$ for SO_4^{2-} and $r^2 = 0.985$ for CrO_4^{2-}. Anion concentration was determined according to USEPA and Standard Methods [25,22]. The pH values of the stabilized/solidified samples were determined using an InoLab Level 2 WTW pH meter and a SenTix 60 glass electrode calibrated with buffer solutions at pH values 4, 7 and 10. Reference solution pH measurements were repeated routinely to check for any drift in pH.

3. Modeling

Two models, the adsorption diffuse layer model (2-pK DLM) and the chemical equilibrium model, were employed to describe the leachability of Zn, Ni, Cu, SO_4^{2-} and CrO_4^{2-} from untreated and S/S waste, in the pH range 2–12.

The DLM cannot distinguish between inner- and outer-sphere complexes [26] and it assumes that all surface complexes are inner-sphere complexes. A diffuse layer of mobile point charges adjoins directly to the surface hydroxyls and complexes in *o*-plane [27]. The diffuse layer initiates at the *d*-plane and extends into the solution phase. The model employs the infinite dilution reference state for the solution and a reference state of zero charge and potential for the surface [28]. The relationship between the surface charge and the surface potential is defined by electric double-layer theory [28,29]. Ionic species adsorption is considered to occur on two types of sites, high-affinity and low-affinity [28]. DLM in the computer program VMINTEQ treats adsorption as a surface complexation reaction (that is, the reaction is treated as analogous to a solution phase complexation reaction governed by a mass action equation) and accounts for the electrostatic potentials at the charged surface [26]. The chemical equilibrium model formulates multiple-component chemical equilibrium problems. The program solves simultaneously the nonlinear mass action expressions and the linear mass balance relationships [30].

The computer program Visual MINTEQ (VMINTEQ ver. 2.3) [26] was used to simulate adsorption, precipitation and aqueous reactions. The Visual MINTEQ is based on the MINTEQA2 (US EPA ver. 4.0) program and it is very similar to it. It utilizes thermodynamic databases, which are largely identical to MINTEQA2 (ver. 4.0), but some additions and changes have been made according to the most recent findings and constants revisions (NIST 46, ver. 6.0 and 7.0). Surface parameters and equilibrium constants used in the DLM adsorption, precipitation and aqueous reactions were provided by the standard databases in the chemical equilibrium program Visual MINTEQ.

4. Results

4.1. Preliminary pH titration test

Useful information about the buffering capacity of the waste and its stabilized/solidified specimens was obtained based on the pH pre-test. The acid buffering capacity of the solidified samples was in every case higher than this of the waste alone (Fig. 1) and lower than that of the cement-binding agent (Fig. 1B). The pH titration curve of untreated oily sludge was conducted using the acid neutralizing capacity (ANC) test (Fig. 1A). The pH measurement of the oily sludge was impossible with the pH

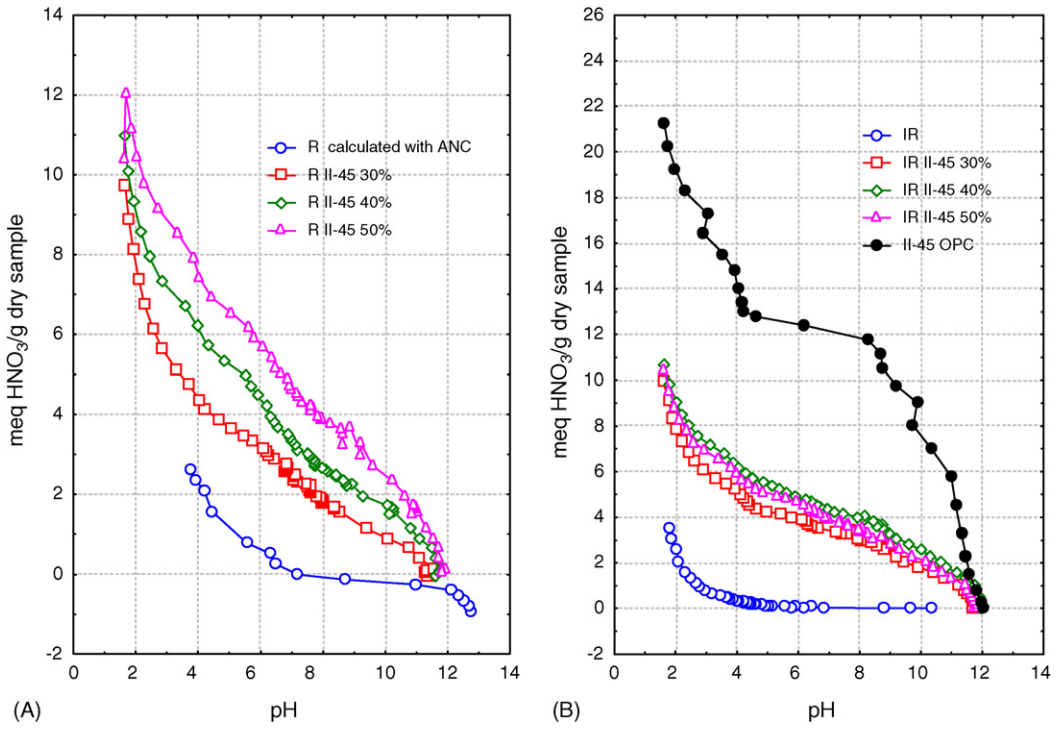

Fig. 1. Preliminary pH titration test of: (A) oily sludge (R) and its S/S specimens, (B) ash (IR) and its S/S specimens, with various amounts of II-45 OPC and II-45 OPC. The negative mequiv. HNO_3 represents the addition of 1 N KOH.

pre-test, because, due to its high content of petroleum hydrocarbons, the sludge had the tendency to form clots after contact with the aqueous medium. As a result, equilibrium could not be reached within the limited contact time (20 min) required by the pH pre-test procedure. On the other hand, the ANC test provided a 48 h contact time with the waste, and equilibrium was reached. The pH titration test showed that solidified oily sludge and ash with II-45 cement increased their buffering capacity as the cement percentage in the specimens increased (Fig. 1). However, the solidified ash did not have the same behavior with solidified sludge. Solidified samples with 40% cement addition had higher buffering capacity than samples with 50% cement addition (Fig. 1B). This behavior was confirmed by duplicate experiment, but no explanation is available.

4.2. Leaching behavior of Zn, Ni and Cu from the oily sludge, ash and their S/S specimens

The effect of II-45 OPC addition to the immobilization of Zn in oily sludge and ash samples is depicted in Fig. 2. In general, oily sludge and its S/S samples leached higher amounts of Zn than the ash and its S/S specimens. Considering the lower initial Zn concentration in oily sludge than in ash (Table 3), it was concluded that the metal was better immobilized in the solidified ash than in the solidified oily sludge. Oily sludge leached the maximum amount at pH 2 (93.2 mg/L in the leachate), whereas the solidified samples leached 30% less Zn at the pH range 2–3.5 (Fig. 2A). The leachability of Zn decreased as the solution became more alkaline. At pH > 7 the leachability of Zn reduced to concentrations less than 1 mg/L. This is indicative of remarkably good Zn immobilization (99.7%) in the cement matrix (Fig. 2C). Solidified samples immobilized Zn better, in the pH range 2–7, than the untreated sludge. This was attributed to the increased amount of ferric hydroxide in the specimen (Table 3). Ferric hydroxide adsorbs Zn on its surface adsorption sites and immobilization of Zn is achieved due to surface complexation. Nevertheless, as the cement addition increased higher leachability of Zn was observed at pH < 6 (Fig. 2C). A possible reason for that was that the cement itself contributed to Zn leaching (Fig. 2A). Maybe, the formation of new solid phases during the hydration and hardening of the cement–waste mixture, favored zinc leachability. The same phenomenon was observed for the solidified ash samples, but only for 50% cement addition (Fig. 2D). Ash and solidified ash with 30% and 40% cement addition showed remarkably good immobilizing characteristics (>90% immobilization of Zn for pH 2–6 and >98% for pH > 6), except for the 50% solidified sample, which, at the pH range 1.6–6.1, showed immobilization of Zn 55–94% (Fig. 2D). The IR II-45 50% sample leached almost 70 mg/L at pH 1.6–4, whereas the leached amount from the remainder of the samples varied from 13.5 to 3.4 mg/L at pH 1.5–5.2 and<0.2 mg/L at pH > 5.2 (Fig. 2B).

On the basis of % immobilization data (Fig. 3), Ni was better stabilized in solidified ash samples compared to solidified oily sludge samples. The oily sludge and S/S sludge samples leached less Ni than ash and S/S ash samples, but the initial concentration in the ash was fourfold the concentration in the sludge. Similarly to Zn, leaching of Ni was higher at pH 2 (9.7 mg/L for solidified oily sludge samples with 50% cement addition) and decreased as the leachate became more basic (1.5 mg/L at pH ≈ 6.8 for all

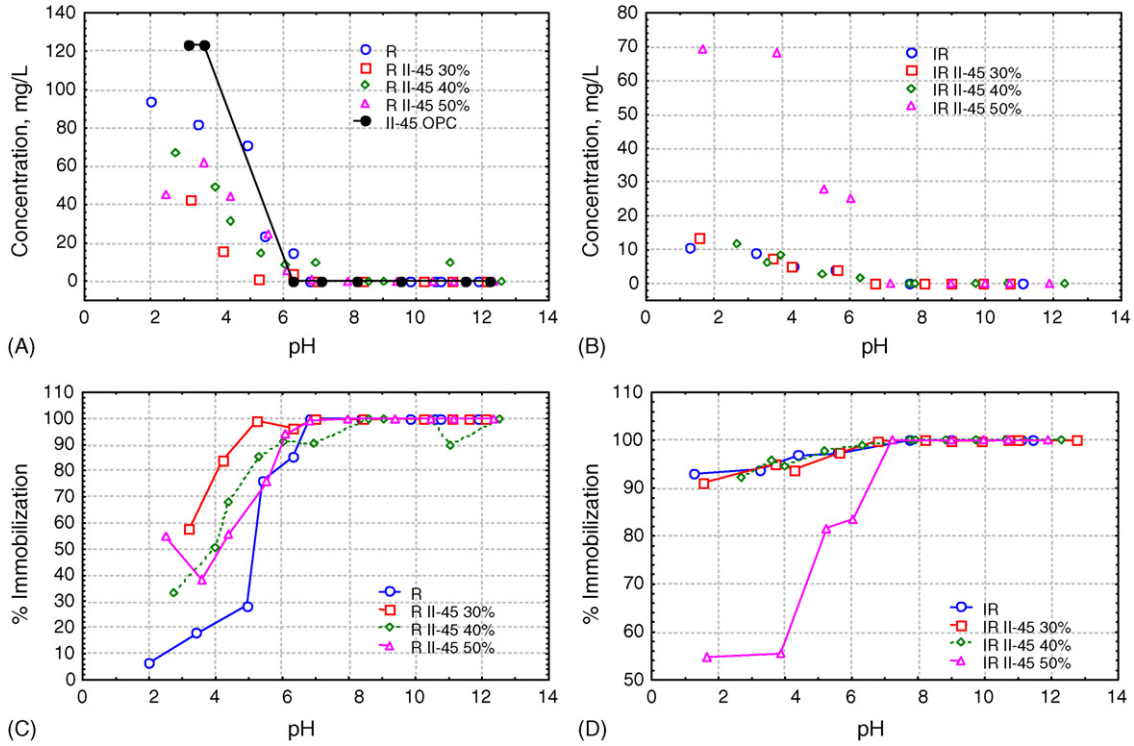

Fig. 2. Zn leaching (mg/L) as a function of pH. (A) From oily sludge and its S/S specimens. (B) From ash and its S/S specimens with II-45 OPC. % Immobilization of Zn as a function of pH. (C) In oily sludge and its S/S specimens. (D) In ash and its S/S specimens.

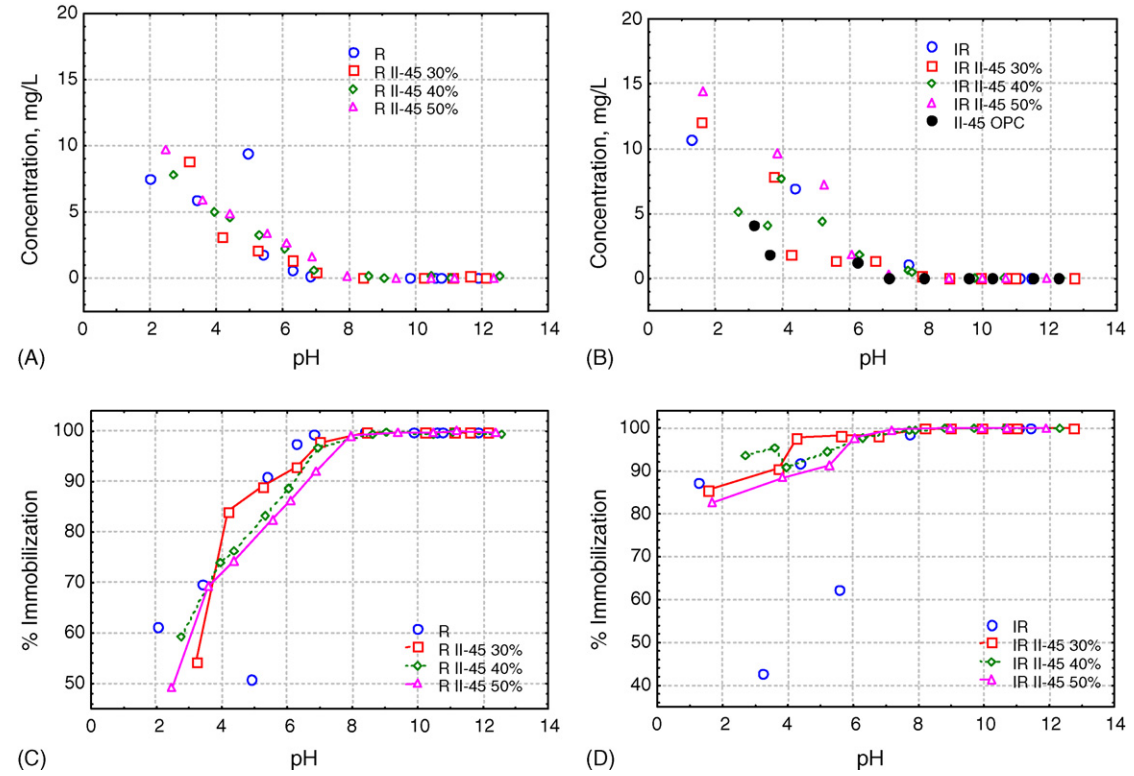

Fig. 3. Ni leaching (mg/L) as a function of pH. (A) From oily sludge and its S/S specimens. (B) From ash and its S/S specimens with II-45 OPC. % Immobilization of Ni as a function of pH. (C) In oily sludge and its S/S specimens. (D) In ash and its S/S specimens.

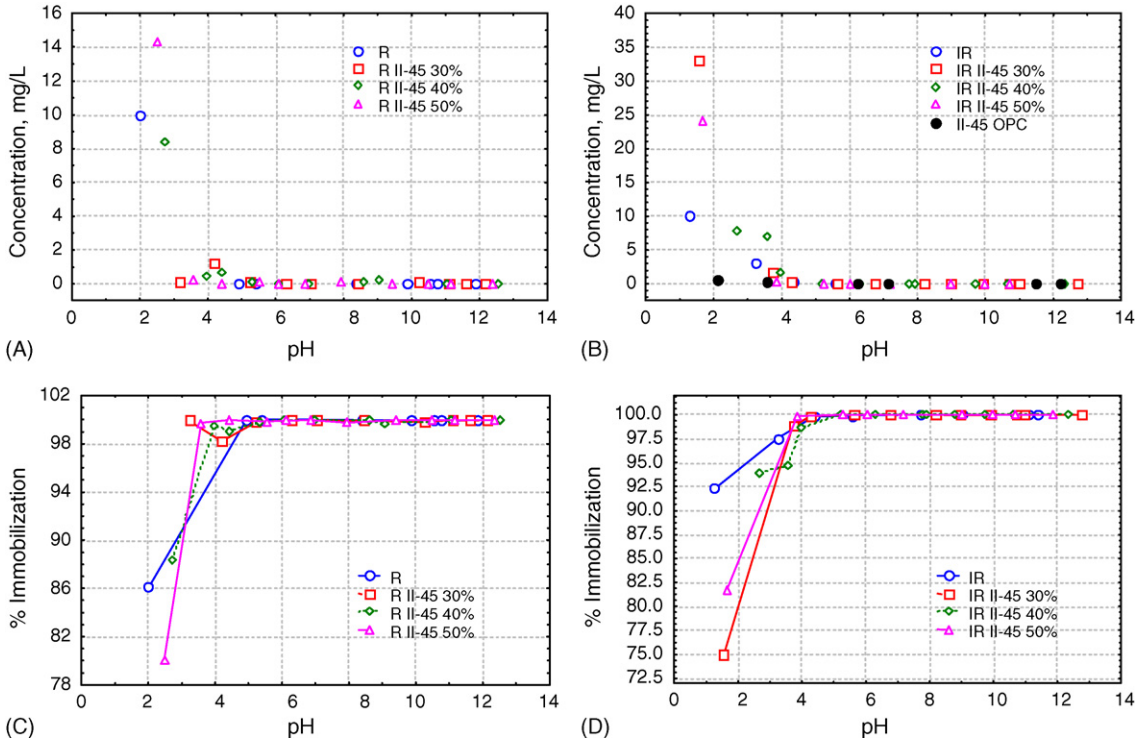

Fig. 4. Cu leaching (mg/L) as a function of pH. (A) From oily sludge and its S/S specimens. (B) From ash and its S/S specimens with II-45 OPC. % Immobilization of Cu as a function of pH. (C) In oily sludge and its S/S specimens. (D) In ash and its S/S specimens.

solidified oily sludge samples) (Fig. 3A). At pH range 6.8–12.6 the release was <0.6 mg/L. On the other hand, Ni release from the ash was very high (47 mg/L at pH 3.2—not shown), whereas the release from solidified ash, at the same pH, was kept low (4–9 mg/L, depending on the amount of cement added) (Fig. 3B). The difference in leaching behavior of Ni between solidified oily sludge and solidified ash was mainly attributed to the buffering capacity of these two types of materials. Solidified ash samples had higher resistance to acid attack, because of the Portlandite concentration into the pore water. Portlandite ($Ca(OH)_2$) controls the pore water pH [27,31]. Fig. 3C shows Ni immobilization in solidified sludge samples. Extremely high immobilization was observed for solidified oily sludge samples with 30%, 40% and 50% cement addition at pH > 8 (>98%), but very low at pH 2.5 (47%), regardless the amount of cement addition. On the contrary, solidified ash samples even at low pH (2–5.5) seemed to immobilize Ni by >80% (Fig. 3D). It was observed that at lower amounts of cement addition the immobilization was more efficient.

The pH titration test showed that copper was remarkably well immobilized in both solidified oily sludge and ash (Fig. 4A and B). This identical leaching behavior may indicate that the same solid phase of Cu controls its leachability. Unlike Zn and Ni, Cu was well stabilized at pH > 3. Above pH 4 immobilization of Cu was 99.5% and 99.8% for solidified sludge and solidified ash, respectively (Fig. 4C and D), regardless of the difference in the initial Cu concentration (Table 3). The maximum Cu leachability was observed at extremely low pH (1.1–2.7), 14.7 mg/L from solidified oily sludge with 50% cement addition and 33 mg/L for solidified ash with 30% cement addition, as indicated in Fig. 4.

4.3. Leaching behavior of SO_4^{2-} and CrO_4^{2-} from the oily sludge, ash and their S/S specimens

Sulfate is an abundant anion in the cement matrix. Many minerals formed during the hydration process and hardening of cement utilize sulfate as a major constituent for their structure. A leaching test with II-45 OPC showed that the cement alone released remarkably high amount of sulfate (from 1500 mg/L at pH of 2 to 2000 mg/L at pH 10) (Fig. 5A and B). Solidification of oily sludge with II-45 OPC showed that at highly alkaline environment (pH 12.4) sulfate was confined in the cement matrix and leaching was reduced to less than 80 mg/L. As the pH decreased, the leachability of sulfate increased dramatically. When the pH reached 9.5 the amount of sulfate leached was at the same level as the II-45 OPC, about 1350 mg/L, for solidified oily sludge with 50% cement addition and for solidified ash with 40% cement addition. At pH < 9.5 sulfate leaching exceeded 1600 mg/L for both types of S/S waste. At pH 2.5–3.4 solidified samples of oily sludge exhibited the maximum sulfate leachability (2034–2310 mg/L for 50% and 30% cement addition, respectively) (Fig. 5A).

An interesting observation was that solidified ash with any percent of cement addition leached less sulfate than the ash or the cement alone, at the pH range from 3 to 11 (Fig. 5B). This means that the mixture of cement and waste created new solid phases more stable and resistant to pH decrease, resulting in lower sulfate release. Worth noticing is the fact that solidified ash with 30% cement addition leached less sulfate than solidified samples with higher percent of cement addition, implying that more additive did not necessarily entail better immo-

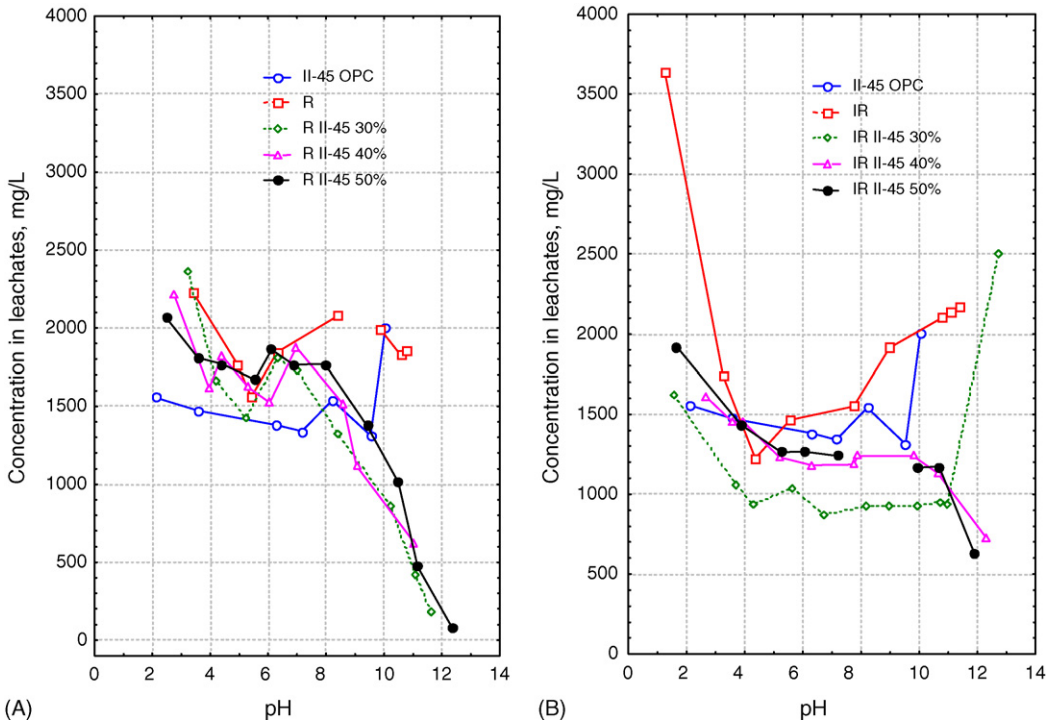

Fig. 5. Sulfate leaching vs. pH from: (A) oily sludge, its S/S specimens and II-45 OPC. (B) Ash, its S/S specimens and II-45 OPC.

bilization. These leaching facts were confirmed by multiple experiments.

However, in the case of chromate leaching, higher percentage of cement resulted in better immobilization of chromate in solidified oily sludge samples compared to those with lower percentage of cement (Fig. 6). It is interesting that no chromate was detected in the leachates of the untreated oily sludge. Nevertheless, chromate leaching behavior of solidified oily sludge was similar to this of the untreated ash. In contrast to solidified oily sludge, solidified ash showed a much better immobilization for chromate compared to the leachability of the untreated ash. In most pH targets, chromate was not detected for solidified ash with 40% and 50% cement addition. Solidified oily sludge samples with 30% cement addition leached more than the other cement mixtures, resulting in chromate concentration in the leachate from 12.4 to 0.18 mg/L at the pH range 1.6–12.7 (Fig. 6).

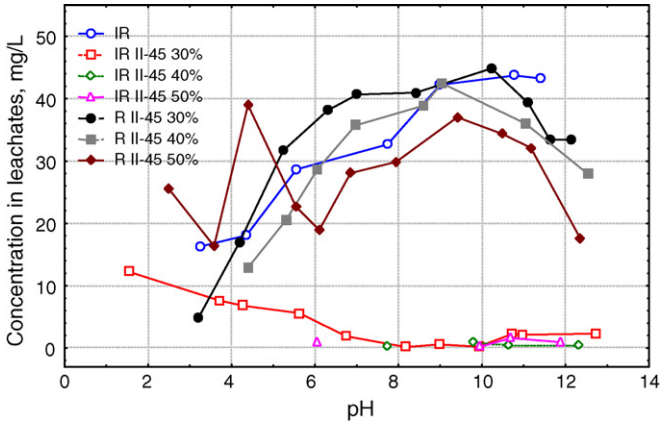

Fig. 6. Chromate leaching (mg/L) from S/S oily sludge specimens, ash and their S/S with II-45 OPC specimens, vs. pH. Chromate leaching from cement was not detected.

4.4. General considerations for modeling Zn, Ni, Cu, SO_4^{2-} and CrO_4^{2-} leaching

The cement matrix and the solid phases formed during stabilization/solidification are very complex. In the modeling simulation, ferrihydrite ($Fe(OH)_3$) was assumed to be the only adsorbent in the solidified waste. For simplicity reasons, it was assumed that Fe of the samples was in the form of ferrihydrite and calculations about concentration were conducted for each waste separately. Thus, for the oily sludge and the S/S sludge samples a solid concentration of 25.23 g $Fe(OH)_{3(s)}$/L leachate was calculated, based on the Fe concentration in the samples. For the ash and the S/S ash samples a solid concentration of 28.92 g $Fe(OH)_{3(s)}$/L leachate was calculated. The presence of iron hydroxides was determined using EXAFS and SEM [32]. The Fe hydroxide is considered to consist of one surface face with two reactive surface site types: singly coordinated ≡FeOH groups which may form surface complexes with anions and/or cationic species (metals), and triply coordinated $\equiv Fe_3O$ groups that do not from surface complexes but nevertheless develop charge [29].

For Zn, Ni, Cu and CrO_4^{2-} the DLM was applied on top of chemical equilibrium, whereas for the SO_4^{2-} chemical equilibrium was adequate to simulate its leachability. Surface and solution parameters considered for the DLM application are listed in Table 4. Two different solid concentrations of ferri-

Table 4
Surface and solution parameters, taken into consideration for the combined DLM and chemical equilibrium application

Surface and solution parameters for ash	Surface and solution parameters for oily sludge
Adsorbent $Fe(OH)_3$ = 28.92 g/L	Adsorbent $Fe(OH)_3$ = 25.23 g/L
Ionic strength = 0.9 M	Ionic strength = 0.9 M
Specific surface area = 600 m^2/g	Specific surface area = 600 m^2/g
Site density = 2.31 sites/nm^2	Site density = 2.31 sites/nm^2
Site concentration (low affinity) = 1.58419	Site concentration (low affinity) = 1.3820
Site concentration (high affinity) = 1.62382	Site concentration (high affinity) = 1.4166
Temperature = 20 °C	Temperature = 20 °C

hydrite for ash and oily sludge solidified samples, respectively, were taken into consideration regarding the iron content in each sample. Site concentration of high and low affinity were calculated by VMINTEQ based on the concentration of adsorbent (ferrihydrite) in each sample. Specific surface parameters, such as specific surface area, were taken from VMINTEQ database, for the specific application of DLM model. The Davies equation [33] was used for activity corrections. Also, oversaturated solids were allowed to precipitate each time a mineral precipitated or dissolved. The temperature was set at 20 °C to better simulate the experimental conditions.

For metals, solid phases such as metal hydroxides and carbonates were mainly assumed, to control their leachability in the increasingly acidic environment of the leaching test. A combination of Cr(VI)Jarosite, Cr(VI)Ettringite, Ettringite, Portlandite, Zincite, $CaCrO_{4(s)}$, $Pb(OH)_{2(s)}$, $Zn(OH)_{2(s)}$, $Cu(OH)_{2(s)}$, $Ni(OH)_{2(s)}$ and $Cu_2SO_{4(s)}$ was applied for the interpretation of cationic and anionic species leachability. Ettringite and Portlandite were identified using XRD and SEM [32]. The other solid phases were inferred on the basis of Cr, Zn, Ni, Cu and SO_4^{2-} chemistry. Surface complexation reactions describing Zn binding to ferrihydrite surface are presented by Eqs. (1) and (2), for Ni Eqs. (3) and (4), whereas Eqs. (5)–(8) present reactions without adsorbed metals. Detailed description of the reactions taken into consideration for modeling Zn leachability is shown in Table 5. Most of the common anions found in the oily sludge and ash were included in the problem setup. Aqueous reactions are presented by Eqs. (9)–(20) for Zn and Eqs. (21)–(28) for Ni. Minerals formed and precipitation reactions are depicted by Eqs. (29)–(47) for Zn, and Eqs. (48)–(53) for Ni. Also, high (marked with "h") and low affinity sites (unmarked) were considered.

Accordingly, detailed description of the reactions taken into consideration for modeling Cu leachability is shown in Table 6. The most important for the simulation are $Cu(OH)_{2(s)}$, $CuSO_{4(s)}$ and $Cu_2SO_{4(s)}$.

For SO_4^{2-} leaching from solidified oily sludge and ash samples, chemical equilibrium was considered as the dominant mechanism, which controlled sulfate leachability. Detailed description of the reactions taken into consideration for modeling sulfate leachability is shown in Table 7. The most important mineral phases for the simulation are Ettringite, Cr(VI)Ettringite, $ZnSO_{4(s)}$ and $Fe_2(SO_4)_{3(s)}$. The presence of

Table 5
Chemical reactions used for simulation of Zn and Ni leachability, using chemical equilibrium and DLM

Reactions		log K[a]
Surface complexation reactions		
$\equiv FehOH^0 + Zn^{2+} = \equiv FehOZn^+ + H^+$	(1)	0.99
$\equiv FeOH^0 + Zn^{2+} = \equiv FeOZn^+ + H^+$	(2)	−1.99
$\equiv FehOH^0 + Ni^{2+} = \equiv FehONi^+ + H^+$	(3)	0.37
$\equiv FeOH^0 + Ni^{2+} = \equiv FeONi^+ + H^+$	(4)	−2.5
$\equiv FehOH^0 + H^+ = \equiv FehOH_2{}^+$	(5)	7.29
$\equiv FehOH^0 = \equiv FehO^- + H^+$	(6)	−8.93
$\equiv FeOH^0 + H^+ = \equiv FeOH_2{}^+$	(7)	7.29
$\equiv FeOH^0 = \equiv FeO^- + H^+$	(8)	−8.93
Aqueous reactions/species		
$Zn^{2+} + 2CO_3{}^{2-} = Zn(CO_3)^{2-}$	(9)	7.3
$Zn^{2+} + 2NO_3{}^- = Zn(NO_3)_{2(aq)}$	(10)	−0.3
$Zn^{2+} + 3H_2O = Zn(OH)_3{}^- + 3H^+$	(11)	−28.391
$Zn^{2+} + 4H_2O = Zn(OH)_4{}^{2-} + 4H^+$	(12)	−41.188
$Zn^{2+} + 2SO_4{}^{2-} = Zn(SO_4)_2{}^{2-}$	(13)	3.28
$2Zn^{2+} + H_2O = [Zn_2(OH)]^{3+} + H^+$	(14)	−8.997
$Zn^{2+} + CO_3{}^{2-} = Zn(CO_3)_{(aq)}$	(15)	4.76
$Zn^{2+} + CO_3{}^{2-} + H^+ = [ZnHCO_3]^+$	(16)	11.829
$Zn^{2+} + NO_3{}^- = [ZnNO_3]^+$	(17)	0.4
$Zn^{2+} + H_2O = [ZnOH]^+ + H^+$	(18)	−8.997
$Zn^{2+} + SO_4{}^{2-} = ZnSO_{4(aq)}$	(19)	2.34
$Zn^{2+} + 2H_2O = Zn(OH)_{2(aq)} + H^+$	(20)	−16.894
$Ni^{2+} + 2H_2O = Ni(OH)_{2(aq)} + 2H^+$	(21)	−18.994
$Ni^{2+} + 3H_2O = [Ni(OH)_3]^- + 3H^+$	(22)	−29.991
$Ni^{2+} + 2SO_4{}^{2-} = [Ni(SO_4)]^{2-}$	(23)	0.82
$Ni^{2+} + SO_4{}^{2-} = NiSO_{4(aq)}$	(24)	2.3
$Ni^{2+} + CO_3{}^{2-} = NiCO_{3(aq)}$	(25)	4.57
$Ni^{2+} + CO_3{}^{2-} + H^+ = [NiHCO_3]^+$	(26)	12.42
$Ni^{2+} + H_2O = [NiOH]^+ + H^+$	(27)	−9.897
$Ni^{2+} + NO_3{}^- = [NiNO_3]^+$	(28)	0.4
Precipitation reactions/minerals		
$Zn^{2+} + SO_4{}^{2-} + 6H_2O$ = Bianchite	(29)	−1.765
$Zn^{2+} + SO_4{}^{2-} + 7H_2O$ = Goslarite	(30)	−2.0112
$5Zn^{2+} + 2CO_3{}^{2-} + 6H_2O$ = Hydrozincite + $6H^+$	(31)	8.7
Zn^{2+} + + $2CO_3{}^{2-}$ = Smithsonite	(32)	−10.9
$Zn^{2+} + H_2O$ = Zincite + $2H^+$	(33)	11.23
$Zn^{2+} + SO_4{}^{2-}$ = Zincosite	(34)	3.9297
$Zn^{2+} + 2NO_3{}^- + 6H_2O = Zn(NO_3)_2{\cdot}6H_2O_{(s)}$	(35)	3.3153
$Zn^{2+} + 2H_2O = Zn(OH)_{2(am)(s)} + 2H^+$	(36)	12.474
$Zn^{2+} + 2H_2O = Zn(OH)_{2(beta)(s)} + 2H^+$	(37)	11.754
$Zn^{2+} + 2H_2O = Zn(OH)_{2(delta)(s)} + 2H^{++}$	(38)	11.844
$Zn^{2+} + 2H_2O = Zn(OH)_{2(epsilon)(s)} + 2H^+$	(39)	11.534
$Zn^{2+} + 2H_2O = Zn(OH)_{2(gamma)(s)} + 2H^+$	(40)	11.734
$2Zn^{2+} + SO_4{}^{2-} + 2H_2O = Zn_2(OH)_2SO_{4(s)} + 2H^+$	(41)	7.5
$3Zn^{2+} + 2SO_4{}^{2-} + H_2O = Zn_3O(SO_4)_{2(s)} + 2H^+$	(42)	18.9135
$4Zn^{2+} + 2SO_4{}^{2-} + 6H_2O = Zn_4(OH)_6SO_{4(s)} + 6H^+$	(43)	28.4
$Zn^{2+} + CO_3{}^{2-} = ZnCO_{3(s)}$	(44)	−10.8
$Zn^{2+} + CO_3{}^{2-} + H_2O = ZnCO_3{\cdot}H_2O_{(s)}$	(45)	−10.26
$Zn^{2+} + SO_4{}^{2-} + H_2O = ZnSO_4{\cdot}H_2O_{(s)}$	(46)	−0.638
$2Zn^{2+} + Al^{3+} + CO_3{}^{2-} + 6H_2O$ = Zn–AlLDH + $6H^+$	(47)	19.83
$Ni^{2+} + SO_4{}^{2-} + H_2O$ = Morenosite	(48)	−2.1449
$Ni^{2+} + 2H_2O = Ni(OH)_{2(am)(s)} + 2H^+$	(49)	12.89
$Ni^{2+} + 2H_2O = Ni(OH)_{2(c)(s)} + 2H^+$	(50)	10.79
$4Ni^{2+} + SO_4{}^{2-} + 6H_2O = Ni_4(OH)_6SO_{4(s)} + 6H^+$	(51)	32
$Ni^{2+} + CO_3{}^{2-} = NiCO_{3(s)}$	(52)	−11.2
$Ni^{2+} + SO_4{}^{2-} + 6H_2O$ = Retgersite	(53)	−2.04

[a] log K were taken from VMINTEQ databases [26].

Table 6
Chemical reactions used for simulation of Cu leachability, using chemical equilibrium and DLM

Reactions		log K[a]
Surface complexation reactions		
$\equiv FeOH^0 + Cu^{2+} = \equiv FeOCu^+ + H^+$	(54)	2.89
$\equiv FeOH^0 + Cu^{2+} = \equiv FeOCu^+ + H^+$	(55)	0.6
$\equiv FeOH^0 + H^+ = \equiv FeOH_2^+$	(56)	7.29
$\equiv FeOH^0 = \equiv FeO^- + H^+$	(57)	−8.93
$\equiv FeOH^0 + H^+ = \equiv FeOH_2^+$	(58)	7.29
$\equiv FeOH^0 = \equiv FeO^- + H^+$	(59)	−8.93
Aqueous reactions/species		
$Cu^{2+} + 2CO_3^{2-} = [Cu(CO_3)_2]^{2-}$	(60)	10.2
$Cu^{2+} + 2NO_3^- = Cu(NO_3)_{2(aq)}$	(61)	−0.4
$Cu^{2+} + 2H_2O = Cu(OH)_{2(aq)} + 2H^+$	(62)	−16.23
$Cu^{2+} + 3H_2O = [Cu(OH)_3]^- + 3H^+$	(63)	−26.64
$Cu^{2+} + 4H_2O = [Cu(OH)_4]^{2-} + 4H^+$	(64)	−39.73
$2Cu^{2+} + 2H_2O = [Cu_2(OH)_2]^{2+} + 2H^+$	(65)	−10.494
$2Cu^{2+} + H_2O = [Cu_2(OH)]^{3+} + H^+$	(66)	−6.71
$3Cu^{2+} + 4H_2O = [Cu_3(OH)_4]^{2+} + 4H^+$	(67)	−20.788
$Cu^{2+} + CO_3^{2-} = CuCO_{3(aq)}$	(68)	6.77
$Cu^{2+} + CO_3^{2-} + H^+ = [CuHCO_3]^+$	(69)	12.129
$Cu^{2+} + SO_4^{2-} + H^+ = [CuHSO_4]^+$	(70)	2.34
$Cu^{2+} + SO_4^{2-} = CuSO_{4(aq)}$	(71)	2.36
$Cu^{2+} + NO_3^- = [CuNO_3]^+$	(72)	0.5
$Cu^{2+} + H_2O = [CuOH]^+ + H^+$	(73)	−7.497
Precipitation reactions/minerals		
$3Cu^{2+} + SO_4^{2-} + 4H_2O$ = Antlerite + $4H^+$	(74)	8.788
$4Cu^{2+} + SO_4^{2-} + 6H_2O$ = Brochantite + $6H^+$	(75)	15.222
$Cu^{2+} + SO_4^{2-} + 5H_2O$ = Chalcanthite	(76)	−2.64
$3Cu^{2+} + 2CO_3^{2-} + 2H_2O$ = Azurite + $2H^+$	(77)	−17.4
$Cu^{2+} + 2H_2O = Cu(OH)_{2(s)} + 2H^+$	(78)	9.29
$2Cu^{2+} + SO_4^{2-} = Cu_2SO_{4(s)}$	(79)	−1.95
$2Cu^{2+} + NO_3^- + 3H_2O = Cu_2(OH)_3NO_{3(s)} + 3H^+$	(80)	9.251
$Cu^{2+} + CO_3^{2-} = CuCO_{3(s)}$	(81)	−11.5
$Cu^{2+} + CrO_4^{2-} = CuCrO_{4(s)}$	(82)	−5.44
$2Cu^{2+} + SO_4^{2-} + H_2O = CuOCuSO_{4(s)} + 2H^+$	(83)	10.3032
$Cu^{2+} + Fe^{3+} + 4H_2O$ = CupricFerrite + $8H^+$	(84)	5.9882
$2Cu^{2+} + H_2O$ = Cuprite + $2H^+$	(85)	−1.406
$Cu^{2+} + Fe^{3+} + 2H_2O$ = CuprousFerrite + $4H^+$	(86)	−8.9171
$Cu^{2+} + SO_4^{2-} = CuSO_{4(s)}$	(87)	2.9395
$4Cu^{2+} + SO_4^{2-} + 7H_2O$ = Langite + $6H^+$	(88)	17.4886
$2Cu^{2+} + CO_3^{2-} + 2H_2O$ = Malachite + $2H^+$	(89)	−5.469
$Cu^{2+} + H_2O = Tenorite_{(am)} + 2H^+$	(90)	8.49
$Cu^{2+} + H_2O = Tenorite_{(c)} + 2H^+$	(91)	7.64

[a] log K was taken from VMINTEQ databases [26].

Table 7
Chemical reactions used for simulation of sulfate leachability, using chemical equilibrium

Reactions		log K[a]
Aqueous reactions/species		
$Al^{3+} + 2SO_4^{2-} = Al(SO_4)_2^-$	(92)	5.58
$Al^{3+} + SO_4^{2-} = Al(SO_4)^+$	(93)	3.84
$Ca^{2+} + SO_4^{2-} = CaSO_{4(aq)}$	(94)	2.36
$2Cr(OH)_2^+ + 2SO_4^{2-} + 2H^+$ = $Cr_2(OH)_2(SO_4)_{2(aq)} + 2H_2O$	(95)	17.9288
$2Cr(OH)_2^+ + SO_4^{2-} + 2H^+$ = $Cr_2(OH)_2SO_4^{2+} + 2H_2O$	(96)	16.155
$CrO_4^{2-} + SO_4^{2-} + 2H^+ = CrO_3SO_4^{2-} + H_2O$	(97)	8.9937
$Cr(OH)_2^+ + SO_4^{2-} + H^+ = Cr(OH)SO_{4(aq)} + H_2O$	(98)	8.2871
$Cr(OH)_2^+ + SO_4^{2-} + 2H^+ = CrSO_4^+ + 2H_2O$	(99)	12.9371
$Cu^{2+} + SO_4^{2-} + H^+ = CuHSO_4^+$	(100)	2.34
$Cu^{2+} + SO_4^{2-} = CuSO_{4(aq)}$	(101)	2.36
$Fe^{3+} + 2SO_4^{2-} = Fe(SO_4)_2^-$	(102)	5.38
$Fe^{3+} + SO_4^{2-} = FeSO_4^+$	(103)	4.05
$SO_4^{2-} + H^+ = HSO_4^-$	(104)	1.99
$Ni^{2+} + 2SO_4^{2-} = Ni(SO_4)_2^{2-}$	(105)	0.82
$Ni^{2+} + SO_4^{2-} = NiSO_{4(aq)}$	(106)	2.3
$Zn^{2+} + 2SO_4^{2-} = Zn(SO_4)_2^{2-}$	(107)	3.28
$Zn^{2+} + SO_4^{2-} = Zn(SO_4)_{(aq)}$	(108)	2.34
Precipitation reactions/minerals		
$4Al^{3+} + SO_4^{2-} + 10H_2O$ = $Al_4(OH)_{10}SO_{4(s)} + 10H^+$	(109)	22.7
$Al^{3+} + SO_4^{2-} + H_2O = Al(OH)SO_{4(s)} + H^+$	(110)	−3.23
$Ca^{2+} + SO_4^{2-}$ = Anhydrite	(111)	−4.36
$Ca^{2+} + SO_4^{2-} + 2H_2O$ = Gypsum	(112)	−4.61
$6Ca^{2+} + 2Al^{3+} + 3SO_4^{2-} + 38H_2O$ = Ettringite + $12H^+$	(113)	56.85
$3Cu^{2+} + SO_4^{2-} + 4H_2O$ = Antlerite + $4H^+$	(114)	8.788
$4Cu^{2+} + SO_4^{2-} + 6H_2O$ = Brochantite + $6H^+$	(115)	15.222
$Cu^{2+} + SO_4^{2-} + 5H_2O$ = Chalcanthite	(116)	−2.64
$2Cu^{2+} + SO_4^{2-} = Cu_2SO_{4(s)}$	(117)	−1.95
$2Cu^{2+} + SO_4^{2-} + H_2O = CuOCuSO_{4(s)} + 2H^+$	(118)	10.3032
$Cu^{2+} + SO_4^{2-} = CuSO_{4(s)}$	(119)	2.9395
$4Cu^{2+} + SO_4^{2-} + 7H_2O$ = Langite + $6H^+$	(120)	17.4886
$Zn^{2+} + SO_4^{2-} + 6H_2O$ = Bianchite	(121)	−1.765
$Zn^{2+} + SO_4^{2-} + 7H_2O$ = Goslarite	(122)	−2.0112
$Zn^{2+} + SO_4^{2-}$ = Zincosite	(123)	3.9297
$Zn^{2+} + SO_4^{2-} + H_2O = ZnSO_4{\cdot}H_2O_{(s)}$	(124)	−0.638
$2Zn^{2+} + SO_4^{2-} + 2H_2O = Zn_2(OH)_2SO_{4(s)} + 2H^+$	(125)	7.5
$3Zn^{2+} + 2SO_4^{2-} + H_2O = Zn_3O(SO_4)_{2(s)} + 2H^+$	(126)	18.9135
$4Zn^{2+} + 2SO_4^{2-} + 6H_2O = Zn_4(OH)_6SO_{4(s)} + 6H^+$	(127)	28.5
$Ni^{2+} + SO_4^{2-} + 7H_2O$ = Morenosite	(128)	−2.1449
$Ni^{2+} + SO_4^{2-} + 6H_2O$ = Retgersite	(129)	−2.04
$4Ni^{2+} + SO_4^{2-} + 6H_2O = Ni_4(OH)_6SO_{4(s)} + 6H^+$	(130)	32
$2Fe^{2+} + 3SO_4^{2-} = Fe_2(SO_4)_{3(s)}$	(131)	−3.7343
$2Fe^{2+} + 2SO_4^{2-} + 7H_2O$ = H-Jarosite + $7H^+$	(132)	−5.39

[a] log K was taken from VMINTEQ databases [26].

Ettringite and possibly $Fe_2(SO_4)_{3(s)}$ was identified using XRD [32]. To achieve better data fits, a small amount of $Fe_2(SO_4)_{3(s)}$ was added to the problem setup, on top of the calculated amount of ferrihydrite. The additional amount of Fe which was considered, for this purpose was only 2.6% of the sum of Fe measured in the ash and II-45 cement.

For chromate leaching from solidified oily sludge and ash, a detailed description of the reactions and surface and solution parameters, which were included in the calculation setup are shown in Table 8. For the interpretation of chromate leaching behavior, chemical equilibrium together with diffuse layer model was employed. Aqueous reactions were considered in the calculations as shown by Eqs. (139)–(146). Precipitation reactions were also included in the model (Eqs. (147)–(154)). Surface parameters used for solidified oily sludge samples were shown in Table 4. Consideration of other anions, such as Cl^- and F^- did not affect the simulation of chromate leaching from the solidified specimens. The main minerals that were included in the model were $CaCrO_4$, Cr(VI)Ettringite, CrO_3, $CuCrO_4$ and $PbCrO_4$. Wang and Vipulanandan [34] have proposed a possible reaction between Cr(VI) and cement, which leads to the

Table 8
Chemical reactions used for simulation of the chromate leachability, using chemical equilibrium and DLM

Reactions		log K[a]
Surface complexations reactions		
$\equiv FeOH^0 + CrO_4^{2-} + H^+ = \equiv FeCrO_4^- + H_2O$	(133)	−7.23
$\equiv FeOH^0 + CrO_4^{2-} = \equiv FeOHCrO_4^{2-}$	(134)	−12.043
$\equiv FehOH^0 + CrO_4^{2-} + H^+ = \equiv FehCrO_4^- + H_2O$	(135)	−7.22
$\equiv FehOH^0 + CrO_4^{2-} = \equiv FehOHCrO_4^{2-}$	(136)	−12.033
$\equiv SOH$	(137)	−8.013
$\equiv SOHh$	(138)	−8.004
Aqueous reactions/species		
$CrO_4^{2-} + Ca^{2+} = CaCrO_{4(aq)}$	(139)	2.77
$2CrO_4^{2-} + 2H^+ = Cr_2O_7^{2-} + H_2O$	(140)	14.56
$CrO_4^{2-} + SO_4^{2-} + H^+ = CrO_3SO_4^{2-} + H_2O$	(141)	8.9937
$CrO_4^{2-} + Fe^{3+} = FeCrO_4^+$	(142)	7.56
$CrO_4^{2-} + 2H^+ = H_2CrO_{4(aq)}$	(143)	6.31
$CrO_4^{2-} + H^+ = HCrO_4^-$	(144)	6.51
$2CrO_4^{2-} + K^+ + 2H^+ = KCr_2O_7^- + H_2O$	(145)	15.32
$CrO_4^{2-} + K^+ = KCrO_4^-$	(146)	0.57
Precipitation reactions/minerals		
$CrO_4^{2-} + Ca^{2+} = CaCrO_{4(s)}$	(147)	−2.2657
$3CrO_4^{2-} + 6Ca^{2+} + 2Al^{3+} + 38H_2O$ = Cr(VI)Ettringite + $12H^+$	(148)	60.29
$CrO_4^{2-} + H^+ = CrO_{3(s)} + H_2O$	(149)	−3.2105
$CrO_4^{2-} + Cu^{2+} = CuCrO_{4(s)}$	(150)	−5.44
$CrO_4^{2-} + Pb^{2+} = PbCrO_{4(s)}$	(151)	−12.6
$2CrO_4^{2-} + K^+ + 3Fe^{3+} + 6H_2O$ = Cr(VI)Jarosite + H^+	(152)	−18.4
$2CrO_4^{2-} + 2K^+ + 2H^+ = K_2Cr_2O_{7(s)} + H_2O$	(153)	−17.2424
$CrO_4^{2-} + 2K^+ = K_2CrO_{4(s)}$	(154)	−0.5134

[a] log K was taken from VMINTEQ databases [26].

formation of $CaCrO_4$. The goodness of fit of all VMINTEQ simulations was based on residual analysis.

4.4.1. Modeling of Zn, Ni and Cu leaching from S/S oily sludge and S/S ash

The leachability of Zn, Ni and Cu (expressed as log C versus pH) was simulated using VMINTEQ. A combination of the solid phases, Mix1: Cr(VI)Jarosite, Cr(VI)Ettringite, Ettringite, Portlandite ($Ca(OH)_2$), Zincite (ZnO), $CaCrO_{4(s)}$, $Pb(OH)_{2(s)}$, $Zn(OH)_{2(s)}$, $Cu(OH)_{2(s)}$, $Ni(OH)_{2(s)}$ and $Cu_2SO_{4(s)}$ was considered to control the total dissolved cationic and anionic species in the leachate. Portlandite was used as a pH adjuster, i.e. to control the pore solution pH. Therefore it was used in all fittings at various concentrations (0.3–5 mM), according the cement percentage in the solidified samples. It was also assumed that the existing amount of Fe (as ferrihydrite) in the oily sludge, ash and II-45 cement played an important role for metal immobilization, by surface complexation onto ferrihydrite *o*-plane.

In the incinerated samples, it was assumed that Zn solubility was controlled by $ZnO_{(s)}$ and/or $Zn(OH)_{2(s)}$. Line 1 (Fig. 7A) represents the total dissolved Zn, when $ZnO_{(s)}$ (Zincite) was the controlling phase. The difference between experimental data and the data calculated by the program was 0.7 log units at pH range 2–5, and 1–1.2 log units at $5 < pH < 9$. A much better simulation was produced, when zinc hydroxide (specifically $Zn(OH)_{2(epsilon)}$) (line 2, Fig. 7A) was considered as the major mineral controlling the leachability of zinc. Other solid phases, such as $ZnCO_{3(s)}$, $ZnO_{(s)}$, $Zn_2(OH)_3Cl_{(s)}$ or $ZnSO_4{\cdot}H_2O_{(s)}$, were also tested, but no combination of these minerals resulted in better agreement with the experimental data. Zinc hydroxide

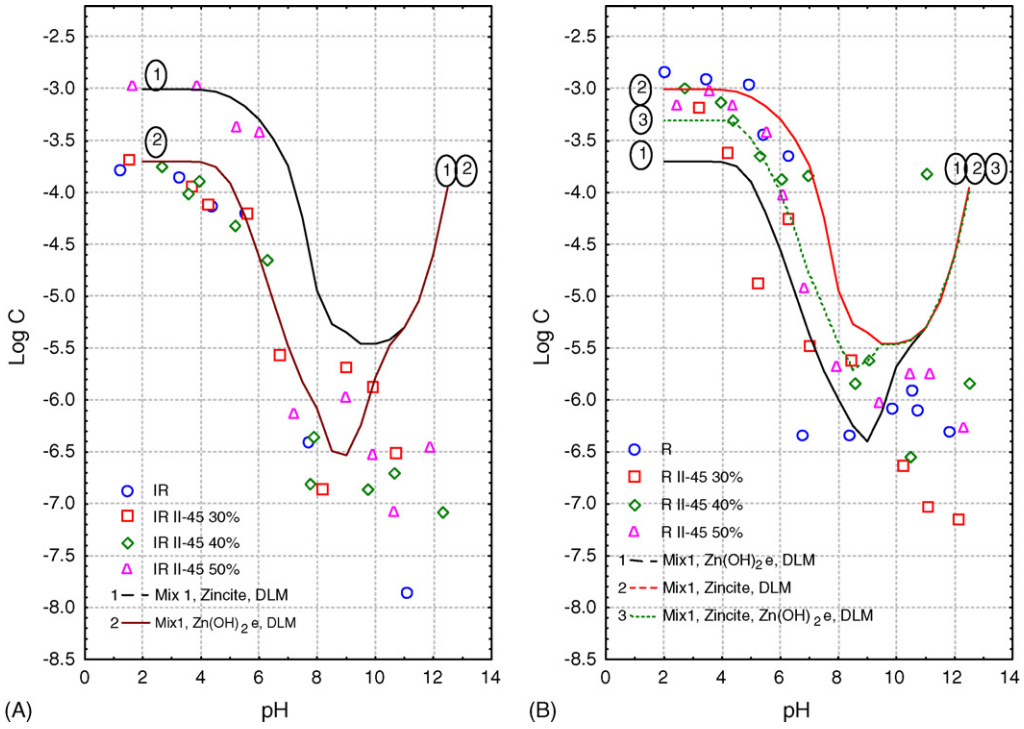

Fig. 7. Comparison of VMINTEQ simulations and experimental data for leaching of Zn vs. pH. (A) S/S ash specimens with various amounts of II-45 Portland cement. (B) S/S oily sludge with various amounts of II-45 Portland cement. Mix1 is described in the text.

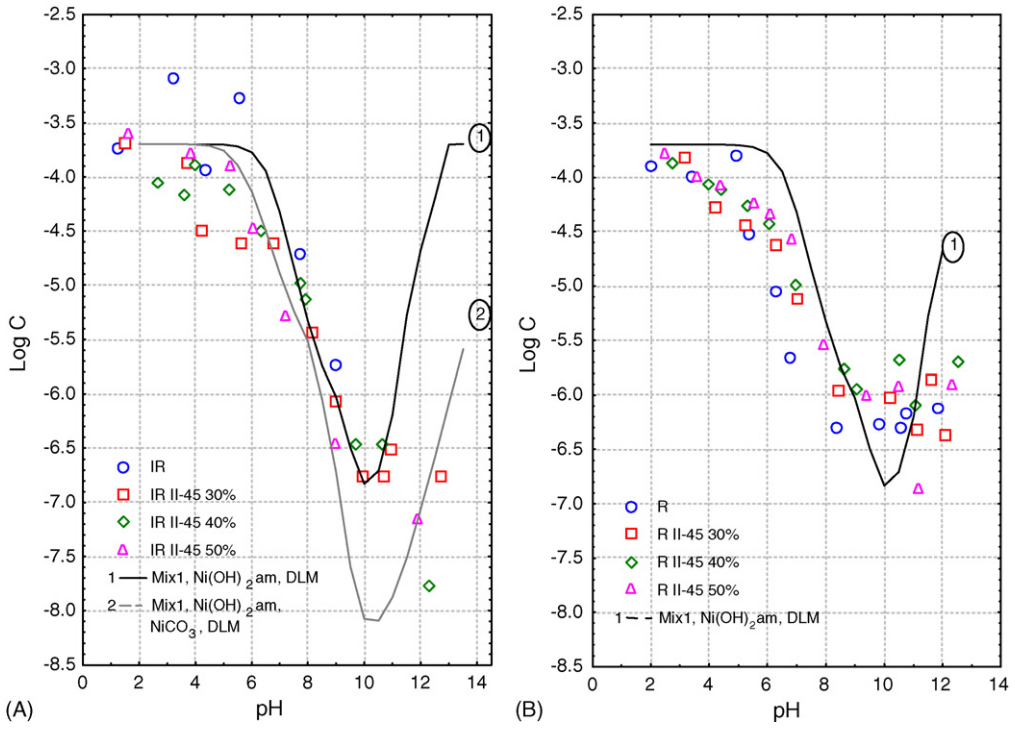

Fig. 8. Comparison of VMINTEQ simulations and experimental data for leaching of Ni vs. pH. (A) S/S ash specimens with various amounts of II-45 Portland cement. (B) S/S oily sludge with various amounts of II-45 Portland cement. Mix1 is described in the text.

dissolution described well the leachability of Zn at pH range from 2 to 10, but it was unable to simulate experimental data at 10 < pH < 12.2 (line 2).

Zinc released from solidified oily sludge was also simulated by $ZnO_{(s)}$ and/or $Zn(OH)_{2(s)}$ (line 2, Fig. 7B). Line 2 (Fig. 7B), which mainly attributed to Zincite dissolution, described well the leached zinc at 2 < pH < 6, but it did not fit the experimental data at pH > 6. Nevertheless, the simulation curve qualitatively fit the leaching trend of dissolved zinc at 2 < pH < 10. Model simulation considering $Zn(OH)_{2(s)}$ alone as the controlling phase resulted in line 1 (Fig. 7B). Solids of Mix1 also contributed to line 1, without any other form of Zn (e.g. ZnO). Considering a combination of $Zn(OH)_{2(s)}$ and $ZnO_{(s)}$ (Zincite) resulted in line 3 (Fig. 7B), which better simulates the experimental data. However, it did not fit the leached zinc at 9 < pH < 12.2. Zinc was expected according to model calculations to dissolve at this pH range, but on the contrary, the experimental results showed that the metal was well immobilized into the cement matrix.

Ni leaching behavior was modeled by surface complexation (DLM 2-pK formalism) in chemical equilibrium state. The same combination of minerals was used as in the case of Zn (namely, Mix1: Cr(VI)Jarosite, Cr(VI)Ettringite, Ettringite, Portlandite, Zincite (ZnO), $CaCrO_{4(s)}$, $Pb(OH)_{2(s)}$, $Zn(OH)_{2(s)}$, $Cu(OH)_{2(s)}$, $Ni(OH)_{2(s)}$ and $Cu_2SO_{4(s)}$). In the incinerated samples, it was assumed that Ni solubility was controlled by $Ni(OH)_{2(am)(s)}$ (line 1, Fig. 8A). The model simulation resulted in remarkably good agreement with the experimental leaching results (line 1, Fig. 8A) at pH range from 1.5 to 11.5. However, at pH 12 the model fit was poor. Several other combinations of minerals were tried, but none was able to simulate the Ni leaching behavior better than line 1 (Fig. 8). An example given in Fig. 8A by line 2, where $NiCO_{3(s)}$ was used in combination with nickel hydroxide, showed that at pH 10.5 the calculated available Ni in solution was less, by 1.6 log units, compared to the experimental results. Line 2 (Fig. 8A) fitted well the leached Ni at pH 12. In line 2 simulation higher amount of Portlandite, than in line 1 (Fig. 8A), was considered. This action resulted in increased buffering capacity of solid matrices which led in decreased total dissolved Ni in the leachate. This lower solubility of Ni-related solid phases described better the experimental data at 5 < pH < 8, but not at 8 < pH < 11.5.

$Ni(OH)_{2(s)}$ was also used as controlling phase to simulate Ni leachability from solidified oily sludge (line 1, Fig. 8B). The experimental results were very close to the calculated dissolved Ni. The similarity in behavior resulted by applying chemical equilibrium and surface complexation using the same combination of solid phases, as in the case of dissolved Ni from solidified ash samples. This was suggestive of similar mechanisms controlling the nickel leaching in solidified specimens.

Copper was one of the most abundant metals found in the oily sludge and, therefore, in the ash samples. A combination of $Cu(OH)_{2(s)}$, $CuSO_{4(s)}$ and monovalent copper in $Cu_2SO_{4(s)}$ was considered to control Cu solubility. The result of VMINTEQ calculations with chemical equilibrium controlling copper dissolution from solidified ash is described by line 1 (Fig. 9A) and demonstrated qualitative agreement with the experimental data, but the fit at pH < 8 was poor. For that reason, DLM considering Cu sorption onto ferrihydrite was applied on top of chemical equilibrium. The new simulation resulted in Line 2 (Fig. 9A), which explained the Cu release reasonably well

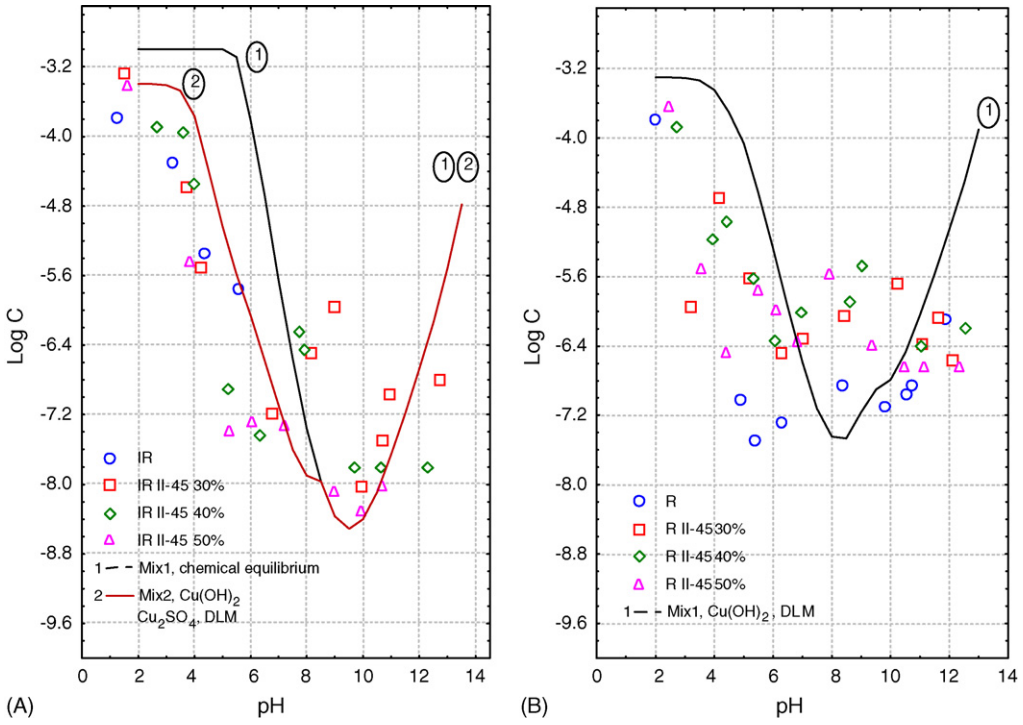

Fig. 9. Comparison of VMINTEQ simulations and experimental data for leaching of Cu vs. pH. (A) S/S ash specimens with various amounts of II-45 Portland cement. (B) S/S oily sludge with various amounts of II-45 Portland cement. Mix1&2 are described in the text.

at the full pH range. The main solid phases that eventually explained Cu leaching behavior from solidified ash were mainly attributed to $Cu(OH)_{2(s)}$ and $Cu_2SO_{4(s)}$. Other mineral species used were Mix1: Cr(VI)Jarosite, Cr(VI)Ettringite, Ettringite, Portlandite, Zincite (ZnO), $CaCrO_{4(s)}$, $Pb(OH)_{2(s)}$, $Zn(OH)_{2(s)}$ and $Ni(OH)_{2(s)}$, the same as in the case of Zn and Ni leaching simulation by VMINTEQ, and Mix2 solid phases, which were the Mix1 solids without Cr(VI)Jarosite and $Zn(OH)_{2(s)}$.

Solidified oily sludge leaching tests resulted in significant experimental data scatter. Nevertheless, the same leaching trend as the one observed in the case of copper leaching from solidified ash was followed (Fig. 9B).

4.4.2. *Modeling of SO_4^{2-} leaching from S/S oily sludge and S/S ash*

Sulfate leachability from solidified oily sludge and ash was simulated using chemical equilibrium as the dominant mechanism controlling sulfate leaching. As it is shown in Fig. 5, the amount of sulfate leaching was high (maximum 2000–2400 mg/L at $2 < pH < 4$ for solidified sludge, and 1600–1900 mg/L at $1.8 < pH < 3$ for solidified ash samples), so the available sulfate in the solidified waste was sufficient to participate in the formation of various cement-related or not, solid phases. A possible mineral formed during hydration of cement or during weathering is Ettringite and Ettringite-related solids (such as Cr(VI)Ettringite) [35,36]. Especially, in excess of sulfate the Ettringite mineral persists and in other cases recrystalizes [37–39]. Also, the presence of organic compounds can contribute to the formation of this mineral. A probable mechanism could include a step where the organic admixture would be concentrated on to the aluminate component, which would increase the reactivity and hence the formation of aluminate products (e.g. Ettringite) [40]. The Ettringite chemistry is well known and it was found that can accommodate several anionic and cationic species into its structure [41,17,18]. Sulfate is an essential structural unit for Ettringite formation. For that reason it was assumed that the major mineral, which controlled sulfate leachability, was Ettringite. Ettringite was found in the solidified oily sludge and ash, among other minerals, using XRD and SEM techniques [32].

For the simulation of sulfate leached from solidified ash samples, Ettringite was considered along with Cr(VI)Ettringite, resulted in line 1 (Fig. 10A). The calculated curve was similar to this of $FeSO_{4(s)}$, Cr(VI)Ettringite, Ettringite and Portlandite (line 2, Fig. 10A), but the experimental results showed a different leaching behavior. The most successful VMINTEQ simulation for leaching of sulfate from the solidified ash with II-45 cement, assumed chemical equilibrium and dominant phases of Ettringite, Portlandite, Zincosite ($ZnSO_{4(s)}$), and $Fe_2(SO_4)_{3(s)}$ (line 3, Fig. 10A). Ettringite was still the dominant mineral, which controlled sulfate release in the aqueous medium, because it had higher concentration than others. $ZnSO_{4(s)}$, and $Fe_2(SO_4)_{3(s)}$ were more soluble at $10 < pH < 13$, whereas Ettringite at the same pH range precipitated. So, at this pH range, sulfate release was controlled by the dissolution of these two minerals, $ZnSO_{4(s)}$, and $Fe_2(SO_4)_{3(s)}$.

Several other minerals used to simulate sulfate leaching resulted in poor fitting to the experimental data.

VMINTEQ calculations for total dissolved sulfate, with Ettringite as the major solid phase, along with Portlandite, and chemical equilibrium as the key mechanism, showed impressive qualitative agreement to experimental results (line 1, Fig. 10B)

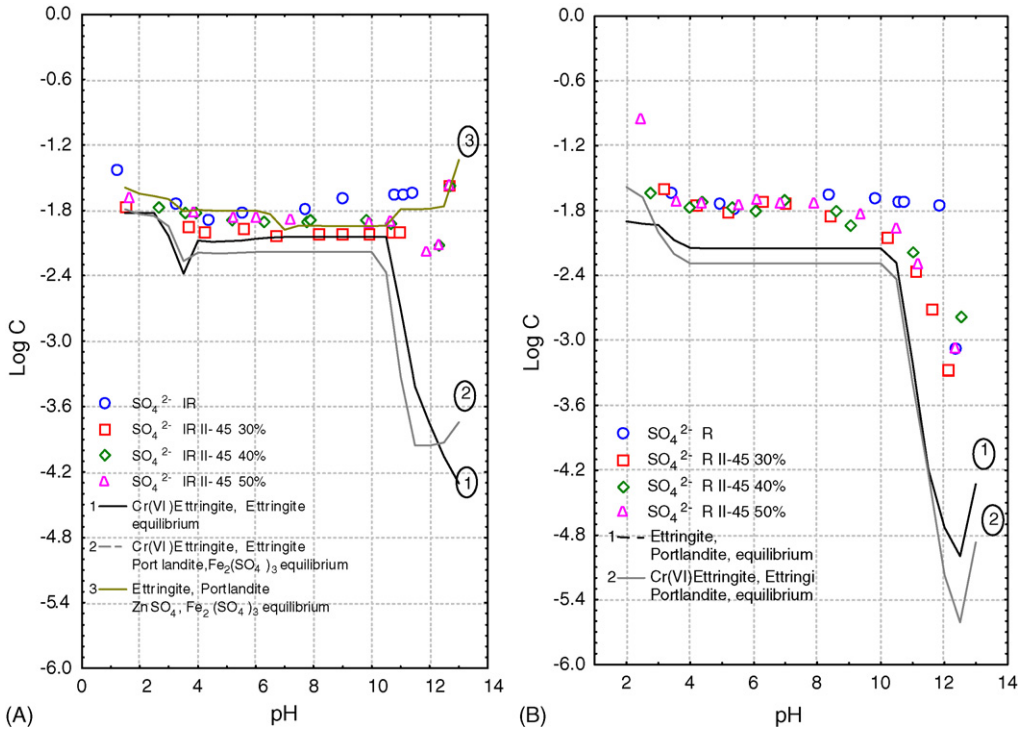

Fig. 10. Comparison of VMINTEQ simulations and experimental data for leaching of SO_4^{2-} vs. pH. (A) S/S ash specimens with various amounts of II-45 Portland cement. (B) S/S oily sludge with various amounts of II-45 Portland cement.

of solidified oily sludge. Nevertheless, at $11 < pH < 13$ the calculated by VMINTEQ sulfate dissolution curve differed from the experimental data by 1.7 log units. Trying to improve the fit, we assumed that substituted Ettringite was present along with common Ettringite as well. The chromate analog was added to the combination of minerals controlling sulfate leachability from solidified oily sludge (line 2, Fig. 10B), and was found to be qualitative similar to line 1 (Fig. 10B). The difference between line 1 and 2 was 0.2 log units at $3.5 < pH < 10.5$ and 0.6 log units at $11.8 < pH < 13$ (Fig. 10B). The same combination was used to simulate sulfate release from solidified ash but still it did not fit the test results (line 1, Fig. 10A).

4.4.3. *Modeling of CrO_4^{2-} leaching from S/S oily sludge and S/S ash*

Chromate was not detected in the leachates of ash and solidified ash samples. The chromate leaching behavior from solidified oily sludge is depicted in Fig. 11. Chemical equilibrium with a surface complexation mechanism was employed for the interpretation of chromate leachability from solidified oily sludge with II-45 cement (Fig. 11). The model took into consideration the heterogeneity of the system by distinguishing low and high affinity sites. The reactions are described by Eqs. (133)–(138) of Table 8. The surface hydroxyl was exchanged by chromate. This surface complex formation is also competitive, because hydroxyl anion and other ligands (chromate) compete for the Lewis acid of the central ion of the ferryhydrate. The extent of surface complex formation (adsorption), is strongly dependent on pH. Since the adsorption of anions is coupled with a release of OH^- ions, adsorption is favored by lower pH values [29]. $CaCrO_{4(s)}$, Cr(VI)Ettringite, Cr(VI)Jarosite and Portlandite were the dominant species considered to control chromate leaching from the solidified oily sludge. Dissolution of $CaCrO_{4(s)}$ was first simulated in the absence of other species considered to exist in the cement matrix. It was assumed [34] to be the possible chromate product during the cement hardening process. Calculations for $CaCrO_{4(s)}$ solubility, based on the VMINTEQ program, showed that at $3 < pH < 10$ the concentration of dissolved CrO_4^{2-} in the solution, was very similar to this of the experimental results (line 1, Fig. 11). For $10 < pH < 12.5$, the difference from the experimental data was larger (0.4 log units).

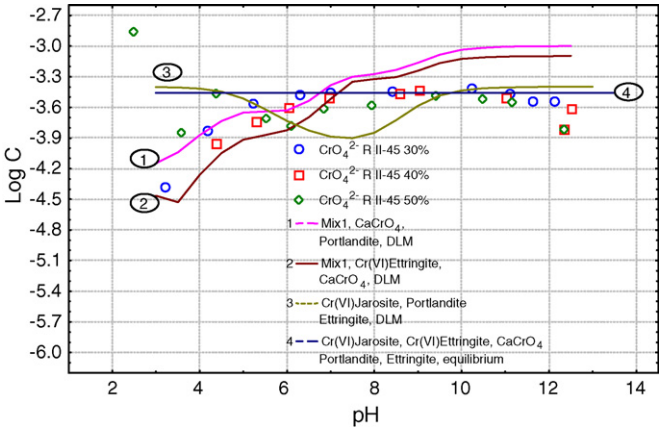

Fig. 11. Comparison of VMINTEQ simulations and experimental data for leaching of CrO_4^{2-} vs. pH, from S/S oily sludge specimens with various amounts of II-45 Portland cement. Mix1 described in the text.

It is common that chromium speciation is dominated by CrO_4^{2-} above pH 8 [20]. The identical charge, similar structure, and comparable thermochemical radii of CrO_4^{2-} and SO_4^{2-} suggest that CrO_4^{2-} could readily substitute for SO_4^{2-} in the crystal structure of many SO_4-minerals, including Ettringite [19], with formation of Cr(VI)Ettringite. The combination of $CaCrO_{4(s)}$ and Cr(VI)Ettringite using DLM, resulted in line 2 (Fig. 11). Dissolution of Cr(VI)Jarosite was also considered as the major mineral which provided the aqueous solution with chromate. DLM was employed and resulted in line 3 (Fig. 11). Reasonably good fitting was obtained by chemical equilibrium of mineral combination containing Cr(VI)Ettringite, Cr(VI)Jarosite, $CaCrO_{4(s)}$, Ettringite and Portlandite, for $5 < pH < 12.5$ (line 4, Fig. 11). Although many more simulations were conducted, lines 1–4 are the ones that best describe the experimental data. The assumption of Cr(VI)Jarosite or $CaCrO_{4(s)}$ as the only solid phase controlling the chromate leaching was not valid and it is not presented in Fig. 11. Chromate leachability was mainly attributed to the dissolution of Cr(VI)Ettringite, Ettringite and $CaCrO_{4(s)}$ modeled by surface complexation (DLM 2-pK formalism) in chemical equilibrium state.

5. Conclusions

In this study, refinery oily sludge and ash produced by incineration of the oily sludge were stabilized/solidified with various additions of II-45 OPC. The solidified waste was tested by means of alkalinity, solubility and release as a function of pH leaching test. The results showed that in oily sludge containing high organic load, pH equilibrium was impossible to be reached with addition of acid or base for the sort contact time required by this leaching test. For cement-matrices containing high organic loaded waste with high heterogeneity, methods, such ANC, which ensure longer contact time with the titrant are more appropriate for the estimation of waste acid buffering capacity. Stabilized/solidified waste was tested for metal and anion leachability, at pH range from 2 to 12. The test revealed that Zn, Ni and Cu leaching was pH-depended. The experiments showed high percent of immobilization (>98%), at $pH > 4$ for Cu, at $pH > 6$ for Zn and $pH > 8$ for Ni, in both sludge and ash solidified with cement. Stabilization/solidification process was more effective, with ash samples, against metal release, considering the initial concentration of metals in each waste. Anion determination showed excessive sulfate leachability from both waste, oily sludge and ash. Chromate was detected only in solidified oily sludge samples.

VMINTEQ was employed to simulate the leaching behavior of the above metals and anions from oily sludge and ash. It was found that the leachability of metals (Zn, Ni and Cu) was controlled by the respective hydroxides and the mechanism which contributed most to metal immobilization was chemical equilibrium and surface complexation, onto ferrihydrite using DLM (2-pK formalism). Zn leached from solidified ash was mainly controlled by the dissolution of $Zn(OH)_{2(epsilon)(s)}$, whereas the metal release from solidified oily sludge was controlled by the combination of $Zn(OH)_{2(epsilon)(s)}$ and $ZnO_{(s)}$, under chemical equilibrium and surface complexation. The same mechanism simulated Ni leachability from both solidified ash and oily sludge samples. $Ni(OH)_{2(am)(s)}$ was the solid phase which most contributed to Ni leaching behavior. In the case of Cu leaching behavior, chemical equilibrium along with surface complexation (DLM) was found to control the Cu release from $Cu(OH)_{2(s)}$ and $Cu_2SO_{4(s)}$ for solidified ash samples. Cu released from solidified oily sludge was attributed to the dissolution of $Cu(OH)_{2(s)}$ using chemical equilibrium along with surface complexation (DLM). Ettringite was the dominant mineral, which controlled sulfate leachability from solidified oily sludge samples and the dominant mechanism considered was chemical equilibrium. Ettringite, along with $ZnSO_{4(s)}$, and $Fe_2(SO_4)_{3(s)}$ played an important role in sulfate leaching from solidified ash samples. Chemical equilibrium with DLM simulation was used to interpret leaching data of chromate. The results showed that Cr(VI)Ettringite, Ettringite and $CaCrO_{4(s)}$, control chromate leachability at the full range of pH. Chemical equilibrium of these solid phases, without surface complexation, was also tried and proved to match chromate leaching data to a certain extend.

References

[1] H.A. van der Sloot, R.N.J. Comans, O. Hjelmar, Similarities in the leaching behaviour of trace contaminants from waste, stabilized waste, construction materials and soils, Sci. Total Environ. 178 (1996) 111–126.
[2] J.A. Stegemann, P.L. Cote, A proposed protocol for evaluation of solidified wastes, Sci. Total Environ. 178 (1996) 103–110.
[3] United States Court of Appeals, Association of Battery Recyclers, Inc., et al., Petitioners v. US Environmental Protection Agency and Carol M. Browner, Administrator, US Environmental Protection Agency, Respondents, No. 98-1368, 1999.
[4] D. Melamed, Monitoring arsenic in the environment: a review of science and technologies with the potential for field measurements, Anal. Chim. Acta 532 (2005) 1–13.
[5] C.S. Poon, K.W. Lio, The limitation of the toxicity characteristic leaching procedure for evaluating cement-based stabilized/solidified waste forms, Waste Manage. 17 (1) (1997) 15–23.
[6] D.S. Kosson, H.A. van der Sloot, F. Sanchez, A.C. Garrabrants, An integrated framework for evaluating leaching in waste management and utilization of secondary materials, Environ. Eng. Sci. 19 (3) (2002) 159–204.
[7] C.A. Johnson, M. Kersten, Solubility of Zn(II) in association with calcium silicate hydrate in alkaline solutions, Environ. Sci. Technol. 33 (13) (1999) 2296–2298.
[8] F. Ziegler, A.M. Scheidegger, C.A. Johnson, R. Dahn, E. Wieland, Sorption mechanisms of zinc to calcium silicate hydrate: X-ray absorption fine structure (XAFS) investigation, Environ. Sci. Technol. 35 (2001) 1550–1555.
[9] F. Ziegler, R. Giere, C.A. Johnson, Sorption mechanisms of zinc to calcium silicate hydrate: sorption and microscopic investigations, Environ. Sci. Technol. 35 (2001) 4556–4561.
[10] C.E. Tommaseo, M. Kersten, Aqueous solubility diagrams for cementitious waste stabilization systems. 3. Mechanism of zinc immobilization by calcium silicate hydrate, Environ. Sci. Technol. 36 (2002) 2919–2925.
[11] J.A. Dyer, P. Trivedi, N.C. Scrinver, D.L. Sparks, Surface complexation modeling of zinc sorption onto ferrihydrite, J. Colloid Interf. Sci. 270 (2004) 56–65.
[12] C. Zhu, Estimation of surface precipitation constants for sorption of divalent metals onto hydrous ferric oxide and calcite, Chem. Geol. 188 (2002) 23–32.

[13] A.M. Scheidegger, E. Weiland, A.C. Scheinost, R. Dahn, P. Spieler, Spectroscopic evidence for the formation of layered Ni–Al double hydroxides in cement, Environ. Sci. Technol. 34 (2000) 4545–4548.
[14] K.G. Karthikeyan, H.A. Elliott, F.S. Cannon, Adsorption and coprecipitation of copper with the hydrous oxides of iron and aluminum, Environ. Sci. Technol. 31 (1997) 2721–2725.
[15] K.G. Karthikeyan, H.A. Elliott, Surface complexation modeling of copper sorption by hydrous oxide of iron and aluminum, J. Colloid Interf. Sci. 220 (1999) 88–95.
[16] R.B. Perkins, C.D. Palmer, Solubility of ettringite ($Ca_6[Al(OH)_6]_2(SO_4)_3{\cdot}26H_2O$) at 5–75 °C, Geochim. Cosmochim. Acta 63 (13/14) (1999) 1969–1980.
[17] I. Baur, P. Keller, D. Mavrocordatos, B. Wehrli, C.A. Johnson, Dissolution–precipitation behavior of ettringite, monosulfate, and calcium silicate hydrate, Cem. Concr. Res. 34 (2004) 341–348.
[18] S.C.B. Myneni, S.J. Traina, T.J. Logan, G.A. Waychunas, Oxyanion behavior in alkaline environments: sorption and desorption of arsenate in ettringite, Environ. Sci. Technol. 31 (1997) 1761–1768.
[19] R.B. Perkins, C.D. Palmer, Solubility of $Ca_6[Al(OH)_6]_2(CrO_4)_3{\cdot}26H_2O$, the chromate analog of ettringite; 5–75 °C, Appl. Geochem. 15 (2000) 1203–1218.
[20] O.E. Omotoso, D.G. Ivey, R. Mikula, Hexavalent chromium in tricalcium silicate. Part I. Quantitative X-ray diffraction analysis of crystalline hydration products, J. Mater. Sci. 33 (1998) 507–513.
[21] F.P. Glasser, Fundamental aspects of cement solidification and stabilization, J. Hazard. Mater. 52 (1997) 151–170.
[22] APHA, AWWA and WEF, in: L.S. Clesceri, A.E. Greenberg, A.D. Eaton (Eds.), Standard Methods for the Examination of Water and Wastewater, 20th ed., APHA, AWWA and WEF, 1998.
[23] USEPA, Acid Digestion of Sediments, Sludges and Soils Method 3050B, is published in "Test Methods for Evaluating Solid Waste, Physical/Chemical Methods", EPA Publication SW-846, December 1996.
[24] J.C. Miller, J.N. Miller, Statistics for Analytical Chemistry, The Method of Standard Additions, 3rd ed., Ellis Horwood/PTR Prentice-Hall, NY, New York, 1993.
[25] USEPA, Determination of Inorganic Anion by Ion Chromatography method 9056, is published in "Test Methods for Evaluating Solid Waste, Physical/Chemical Methods", EPA Publication SW-846, July 1992.
[26] J.P. Gustafsson, Visual MINTEQ ver, 2.30, KTH Royal Institute of Technology, Sweden, 2004.
[27] A.P. Robertson, J.O. Leckie, Cation binding predictions of surface complexation models: effects of pH, ionic strength, cation loading, surface complex and model fit, J. Colloid Interf. Sci. 188 (1997) 444–472.
[28] S. Goldberg, Use of surface complexation models in soil chemical systems, Adv. Agron. 47 (1993) 233–329.
[29] W.W. Stum, J.J. Morgan, Aquatic Chemistry: Chemical Equilibria and Rates in Natural Waters, third ed., Wiley/Interscience Publication, NY, New York, 1996.
[30] MINTEQA2/PRODEFA2, A Geochemical Assessment Model for Environmental Systems: Version 3.0 User's Manual, Athens, Georgia, US EPA/600/3-91/021, 1991.
[31] R.J. van Eijk, H.J.H. Brouwers, Modelling the effects of waste components on cement hydration, Waste Manage. 21 (2001) 279–284.
[32] A.K. Karamalidis, Management of refinery oily sludge using stabilization/solidification: leachability and immobilization mechanisms of metals, anions and hydrocarbons, PhD Thesis, 2006.
[33] F.M.M. Morel, J.G. Hering, Principles and Applications of Aquatic Chemistry, Wiley/Interscience Publication, NY, New York, 1993.
[34] S. Wang, C. Vipulanandan, Solidification/stabilization of Cr(VI) with cement. Leachability and XRD analyses, Cem. Concr. Res. 30 (2000) 385–389.
[35] C.D. Palmer, Precipitates in a Cr(VI)-contaminated concrete, Environ. Sci. Technol. 34 (2000) 4185–4192.
[36] S.C.B. Myneni, S.J. Traina, T.J. Logan, Ettringite solubility and geochemistry of the $Ca(OH)_2$–$Al_2(SO_4)_3$–H_2O system at 1 atm pressure and 298 K, Chem. Geol. 148 (1998) 1–19.
[37] J. Skanly, J. Marchand, I. Odler, Sulfate Attack on Concrete, Spon Press, NY, New York, 2002.
[38] S. Diamond, Delayed ettringite formation—processes and problems, Cem. Concr. Compos. 18 (1996) 205–215.
[39] L. Divet, R. Randriambololona, Delayed ettringite formation: the effect of temperature and basicity on the interaction of sulphate and C–S–H phase, Cem. Concr. Res. 28 (3) (1998) 357–363.
[40] D.M. Montgomery, C.J. Sollars, R. Perry, S.E. Tarling, P. Barnes, E. Henderson, Treatment of organic-contaminated industrial wastes using cement-based stabilization/solidification. I. Microstructural analysis of cement–organic interactions, Waste Manage. Res. 9 (1991) 103–111.
[41] M.L.D. Gougar, B.E. Scheetz, D.M. Roy, Ettringite and C–S–H Portland cement phases for waste ion immobilization: a review, Waste Manage. 16 (4) (1996) 295–303.